e-ISSN: 2689-4934

Available online at
http://uppp.uitm.edu.my/online-issues.html

ESTEEM Academic Journal Vol 21, March 2025, 59-73

ESTEEM **Academic Journal (EAJ)**

Influence of iron doping on the morphological and compositional properties of zirconia foil as photocatalyst

Nor Aimi Abdul Wahab[1], Adhwa Izzati Md Taib[2], Nabilah Yasmin Shamsol Afandi[2], Norain Isa[2,3*], Nurulhuda Bashirom[4], Mustaffa Ali Azhar Taib[5], Zainovia Lockman[6]

[1]*Department of Applied Sciences, Universiti Teknologi MARA, Cawangan Pulau Pinang, 13500 Permatang Pauh, Pulau Pinang, Malaysia*
[2]*Chemical Engineering Studies, Universiti Teknologi MARA, Cawangan Pulau Pinang, 13500 Permatang Pauh, Pulau Pinang, Malaysia*
[3]*Waste Management and Resource Recovery (WeResCue) Group, Chemical Engineering Studies, College of Engineering, Universiti Teknologi MARA, Cawangan Pulau Pinang, 13500 Permatang Pauh, Pulau Pinang, Malaysia*
[4]*School of Materials Engineering, Kompleks Pusat Pengajian Jejawi 2, Universiti Malaysia Perlis, Taman Muhibbah, 02600 Jejawi, Arau, Perlis, Malaysia*
[5]*Division of Advanced Ceramic Materials Technology, Advanced Technology Training Center (ADTEC) Taiping, 34600, Kamunting, Perak, Malaysia*
[6]*School of Materials and Mineral Resources Engineering, Engineering Campus, Universiti Sains Malaysia, 14300 Nibong Tebal, Pulau Pinang, Malaysia*

ARTICLE INFO

Article history:
Received 15 January 2025
Revised 27 February 2025
Accepted 10 March 2025
Online first
Published 24 March 2025

Keywords:
Iron doping
Zirconia
Photocatalyst
Morphological
Compositional

*DOI:*10.24191/esteem.v21iMarch.586.g3074

ABSTRACT

Zirconia (ZrO_2) is a promising photocatalyst; however, its performance is often limited by poor charge separation and low visible light absorption. To enhance its photocatalytic potential, this study investigates the effects of iron doping on the morphology and composition of zirconia foil. Iron(II) sulfate heptahydrate ($FeSO_4 \cdot 7H_2O$) and iron(III) nitrate nonahydrate ($Fe(NO_3)_3 \cdot 9H_2O$) were used at varying concentrations to examine their effects through scanning electron microscopy (SEM) and energy-dispersive X-ray spectroscopy (EDX). The findings reveal that higher concentrations of both irons induce notable surface restructuring compounds that cause considerable surface changes and color variations, indicating successful doping among the two precursors, $Fe(NO_3)_3 \cdot 9H_2O$ exhibits superior doping efficiency at lower concentrations. This study provides qualitative insights into these morphological modifications, contributing to a better understanding of iron-doped zirconia's role in photocatalysis.

[1*] Corresponding author. *E-mail address*: norain012@uitm.edu.my
https://doi.org/10.24191/esteem.v21iMarch.586.g3074

1. INTRODUCTION

Zirconia (ZrO_2) is known for its chemical stability, wear resistance, and strong mechanical properties [1]. These qualities have made it useful in various applications, including biomedical implants, dental prostheses, industrial equipment, and heat barrier coatings [2]. Furthermore, its high ionic conductivity makes it essential in solid oxide fuel cells and oxygen sensors, while its optical characteristics permit use in optical fibers and lenses [3]. Doping, a critical strategy in materials research, entails introducing trace amounts of foreign elements to improve material features [4]. This procedure changes zirconia's electrical conductivity, mechanical strength, and thermal stability, making it more suitable for specific applications.

Leib's group revealed that yttrium-doped zirconia exhibits higher thermal stability, making it appropriate for high-temperature applications [5]. Similarly, Deng's group [6] proved that Ce-Zr-based materials possess good thermal stability and outstanding low-temperature reducibility, further expanding zirconia's potential applications.

Iron doping in ZrO_2 has gained attention for its considerable impact on electrical, magnetic, and optical properties. De Souza's group [7] demonstrated that iron doping modifies zirconia's grain size and surface morphology, directly influencing its mechanical and thermal properties, which are critical for advanced technological applications. Similarly, Doufar's group [8] found that heat treatment improves the photocatalytic performance of Fe-doped ZrO_2, highlighting the impact of doping and processing conditions.

Photocatalysts, such as ZrO_2, play a significant role in wastewater treatment by degrading contaminants. Bashirom's group [9] found that iron-doped zirconia, especially after anodization, outperforms undoped ZrO_2 in removing organic pollutants. Anodization, a widely used technique in materials science, has been extensively researched for its potential to change the structural, chemical, and electrical properties of numerous materials, particularly metals and ceramics [10]–[12]. Similarly, studies on nanoparticles synthesized via green methods have demonstrated highly effective catalytic activity in dye degradation, highlighting the potential of nanomaterials in wastewater purification [13].

Table 1 outlines the various applications of pure and modified ZrO_2. While zirconia's inherent qualities make it appropriate for biomedical and industrial applications, iron doping enhances its mechanical and catalytic performance. This modification enables its use in high-temperature environments, durable implants, and catalytic processes. Iron-doped ZrO_2 exhibits increased electrical and photocatalytic capabilities, making it viable for environmental applications, especially in wastewater treatment technologies.

This work examines how iron doping affects the morphological and compositional features of ZrO_2, specifically its photocatalytic capability in wastewater treatment. This study investigates how iron incorporation, specifically through anodization, affects the structural and surface characteristics of ZrO_2. Previous research, such as that of Reddy's group [23], has shown that iron doping improves photocatalytic activity by increasing surface area and defect sites. This study aims to contribute to the development of more efficient and effective photocatalytic materials for environmental applications.

https://doi.org/10.24191/esteem.v21iMarch.586.g3074

Table 1: Application of zirconia and modified zirconia

Attribute	Zirconia (ZrO_2)	Iron-Doped Zirconia
Biomedical applications	Used in dental implants, crowns, hip and knee replacements due to biocompatibility and strength [1].	Improved mechanical and wear properties enhance its suitability for long-lasting biomedical implants [14].
Industrial uses	Employed in cutting tools, bearings, and thermal barrier coatings owing to wear resistance and thermal stability [15].	Enhanced properties may improve performance in similar industrial applications [16].
Ceramics and refractories	Common in high-temperature applications due to high melting point and low thermal conductivity [17]	Potential for improved performance in high-temperature environments [18].
Oxygen sensors and fuel cells	Utilized for oxygen ion conductivity in high temperatures in oxygen sensors and solid oxide fuel cells (SOFCs) [3].	Modified electrical properties may enhance fuel cell and sensor efficiency [19].
Catalysis	Good performance as photocatalyst [12].	Enhanced catalytic properties make it useful in chemical reactions, such as exhaust gas treatment in the automotive industry [20].
Energy storage and conversion	Limited use in energy storage and conversion.	Improved electrical properties may improve performance in energy conversion devices like fuel cells and batteries [21].
Environmental applications	Limited use in environmental applications.	Used in photocatalysis for water purification and air cleaning due to enhanced photocatalytic activity [9].
Electronics and photonics	Limited use in electronics and photonics.	Sensors and optical fibers can leverage altered electrical and optical properties [22].

2. METHODOLOGY

2.1 Sample Preparation

Zirconium (Zr) foils, 0.05 mm in thickness and with a purity of 99.8% (sourced from Nilaco Corporation, Japan), were cut into dimensions of 1 cm × 4 cm. These foils were cleaned ultrasonically in acetone and ethanol, then rinsed with distilled water and air-dried.

2.2 Anodization Process

The anodization was carried out in a custom electrolyte mixture, following the method by Isa et al. [10], [24]. This mixture consisted of 80 mL ethylene glycol (EG), 0.3 wt% ammonium fluoride (NH_4F), and iron-containing compounds. Two types of iron compounds were used in separate trials: iron (II) sulfate heptahydrate ($FeSO_4.7H_2O$) and iron (III) nitrate nonahydrate ($Fe(NO_3)_3.9H_2O$). Each iron compound was introduced in varying concentrations (0.1, 0.5, and 1.0 M) to study their effects on the zirconia foil.

The electrochemical setup for the anodization involved the Zr foil as the anode and platinum as the cathode placed 30 mm apart. The anodization was conducted at 60 V for 1 h. A bubbling system was utilized to stir the electrolyte during the process. Post-anodization, the Zr foils were removed from the electrolyte, rinsed with distilled water, air-dried, and annealed at 500 ºC. A summary of the preparation and anodization of Zr foil is shown in Fig. 1.

https://doi.org/10.24191/esteem.v21iMarch.586.g3074

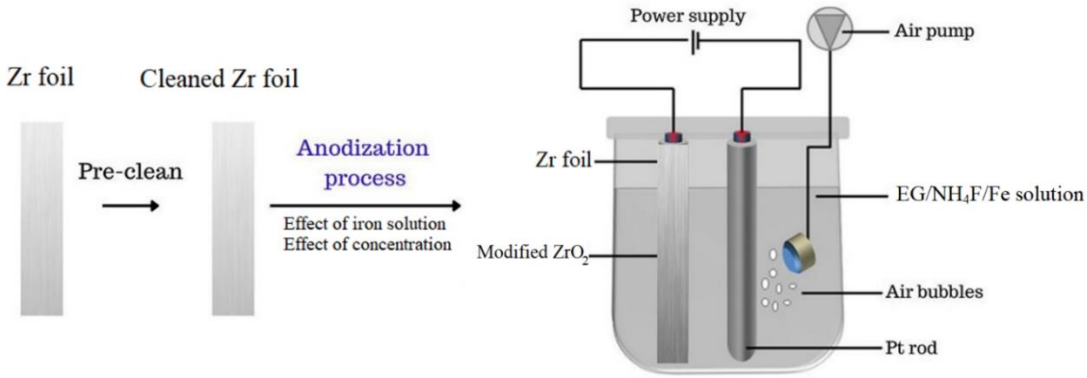

Fig. 1: Summarization of synthesis of iron-modified zirconia

2.3 Characterization of Modified Zirconia

The morphological and compositional characteristics of the anodized and annealed ZrO_2, along with the iron-doped ZrO_2 nanotubes, were analyzed using field emission scanning electron microscopy (FESEM; variable pressure, Zeiss Supra 35) and energy dispersive X-ray (EDX). These techniques were employed to assess the effects of both types of iron doping on the zirconia's structure and composition.

3. RESULTS AND DISCUSSION

3.1 Morphological and Compositional of ZrO_2 and Iron Modified ZrO_2

In this study, ZrO_2 was modified using two different iron compounds at varying concentrations, leading to notable changes in its physical appearance. Specifically, the modifications involved doping with iron (II) sulfate heptahydrate ($FeSO_4.7H_2O$) and iron (III) nitrate nonahydrate ($Fe(NO_3)_3.9H_2O$) at concentrations of 0.1, 0.5, and 1.0 M.

Based on the visual observation in Fig. 2, for ZrO_2 doped with 0.1 M (Fig. 2 (a)) of $FeSO_4.7H_2O$, the changes in appearance were subtle, reflecting the lower concentration of the doping agent. As the concentration increased to 0.5 M (Fig. 2 (b)), these modifications became more pronounced, indicating a more significant alteration in the surface morphology and coloration of the ZrO_2. At the highest concentration of 1.0 M (Fig. 2 (c)) of $FeSO_4.7H_2O$, the ZrO_2 exhibited the most noticeable changes, likely showing a darker coloration and distinct textural differences due to the higher level of iron incorporation. Similarly, the visual impact of doping ZrO_2 with iron (III) nitrate followed a comparable trend. At the lower concentration of 0.1 M (Fig. 2 (d)) of $Fe(NO_3)_3.9H_2O$, minimal changes were observed. However, as the concentration increased to 0.5 M (Fig. 2 (e)) and further to 1.0 M (Fig. 2 (f)), the ZrO_2 displayed more evident modifications. These higher concentrations of $Fe(NO_3)_3.9H_2O$ likely resulted in more pronounced color changes and morphological alterations in the ZrO_2, showcasing the effect of iron concentration on the material's physical characteristics.

These observations align with findings from Chen's group [25], where enhanced dopant concentrations in similar oxide materials were found to alter physical characteristics significantly. The higher iron concentrations likely resulted in more pronounced color changes and morphological alterations in the ZrO_2, showcasing the effect of iron concentration on the material's physical characteristics.

https://doi.org/10.24191/esteem.v21iMarch.586.g3074

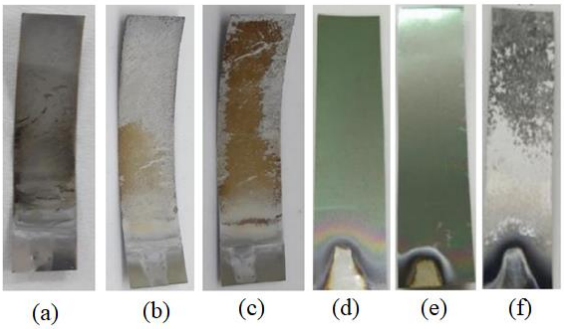

Fig. 2: Visual images of zirconia modified with (a) 0.1 M of $FeSO_4.7H_2O$, (b) 0.5 M of $FeSO_4.7H_2O$ (c) 1.0 M of $FeSO_4.7H_2O$ (d) 0.1 M of $Fe(NO_3)_3.9H_2O$, (e) 0.5 M of $Fe(NO_3)_3.9H_2O$ and (f) 1.0 M of $Fe(NO_3)_3.9H_2O$

SEM is a powerful tool widely used in various fields to understand the surface composition and morphology of different materials. In the SEM images provided in Fig. 3, it was observed that the distinct effects of doping ZrO_2 with different concentrations of iron (II) sulfate heptahydrate ($FeSO_4.7H_2O$) and iron (III) nitrate nonahydrate ($Fe(NO_3)_3.9H_2O$) on its surface morphology. An interesting feature was observed in the SEM images where ZrO_2 was doped with varying concentrations of $FeSO_4.7H_2O$, as shown in Fig. 3 (a) – (c). Alongside the formation of ZrO_2 nanotubes, the surfaces of these nanotubes appear to be covered with clusters or agglomerations. This phenomenon is particularly noticeable at higher doping concentrations. The presence of these agglomerations on the surface of ZrO_2 nanotubes could be attributed to several factors. It might result from the coalescence of smaller particles during the doping process, forming larger, irregularly shaped aggregates. Such behavior is standard in nanoparticle synthesis and has been observed in other studies [26], [27].

For instance, Xu's group reported similar occurrences where increased dopant concentrations led to particle agglomeration on the surfaces of modified nanomaterials [28]. These agglomerations could potentially impact the properties and applications of the ZrO_2 nanotubes. While they might increase the overall surface area [29], which is beneficial for applications like catalysis or adsorption, they could also interfere with the uniformity and consistency of the tube surfaces. This, in turn, could affect the material's performance in specific applications.

Similar observations are made when doping ZrO_2 with iron (III) nitrate nonahydrate ($Fe(NO_3)_3.9H_2O$), as shown in Fig. 3 (d) – (f). At lower concentrations, only subtle modifications are seen in the SEM images, but as the concentration increases to 0.5 M and further to 1.0 M, the SEM images reveal more pronounced morphological transformations. These changes include more evident surface structure alterations, such as grain size and texture variations, indicating a stronger influence of iron doping. However, unlike the modifications observed with $FeSO_4.7H_2O$, the doping of ZrO_2 with $Fe(NO_3)_3.9H_2O$ did not form nanotubes. Instead, the SEM images show the presence of clumps or agglomerations on the surface. This could indicate a different interaction mechanism between the zirconia matrix and the iron (III) nitrate, leading to a distinct morphological outcome. The formation of these clumps or agglomerations suggests a possible aggregation of zirconia particles or a localized concentration of the iron dopant on the surface. Such a phenomenon is noteworthy and aligns with the findings of Fletcher's group [30], which reported that increased concentrations of certain dopants in oxide materials could lead to significant surface agglomerations rather than the formation of structured nanoforms like nanotubes. These agglomerations could affect the material's properties, such as potential agglomerations affecting its catalytic activity, surface reactivity, or mechanical

https://doi.org/10.24191/esteem.v21iMarch.586.g3074

strength. The fact that no nanotubes were observed in the case of $Fe(NO_3)_3.9H_2O$ doping highlights the complexity of material behavior under different doping conditions. It underscores the importance of dopant selection in tailoring the morphological and functional properties of materials like ZrO_2.

These findings align with previous research, such as Cheng et al. [30], who studied Fe-doped zirconia nanoparticles and found that the concentration and type of iron precursor substantially influence the conduction band potential, boosting photocatalytic efficiency. The study found that adding Fe to ZrO_2 improves visible-light photocatalysis and modifies electrical characteristics, explaining the observed iron uptake disparities. Similarly, Jelaini et al. [9] investigated the anodic oxidation of Zr-5Fe alloys, finding that iron was essential in changing surface chemistry and electrochemical behavior, ultimately enhancing Cr(VI) elimination under sunlight. Their findings support that iron doping can affect the structural and electrical properties of Zr-based materials depending on the precursor type and concentration.

Fig. 4, Fig. 5, and Table 1 show EDX analysis of ZrO_2 doped with $FeSO_4 \cdot 7H_2O$ and $Fe(NO_3)_3 \cdot 9H_2O$, revealing elemental composition changes. Lower quantities of ZrO_2-$FeSO_4 \cdot 7H_2O$ typically contain carbon, oxygen, fluorine, and zirconium, with zirconium being the main component. As the concentration increases, there is a distinct drop in carbon and oxygen, but fluorine content increases and iron become detectable at 1.0 M, indicating that effective doping occurs at greater concentrations. In contrast, ZrO_2-$Fe(NO_3)_3 \cdot 9H_2O$ reveals the presence of iron even at lower concentrations, suggesting that $Fe(NO_3)_3 \cdot 9H_2O$ supports a more efficient doping process, as indicated in fluctuations in nitrogen and oxygen content. Furthermore, the earlier presence of Fe in the nitrate-based solution compared to the sulfate-based one indicates a more efficient iron incorporation process. Higher fluorine concentrations in the sulfate solution may be due to the interaction between sulfate ions and ZrO_2, which affects doping efficiency. These changes in elemental composition substantially impact the material's physical and chemical properties, influencing its appropriateness for applications such as photocatalysis and environmental restoration.

https://doi.org/10.24191/esteem.v21iMarch.586.g3074

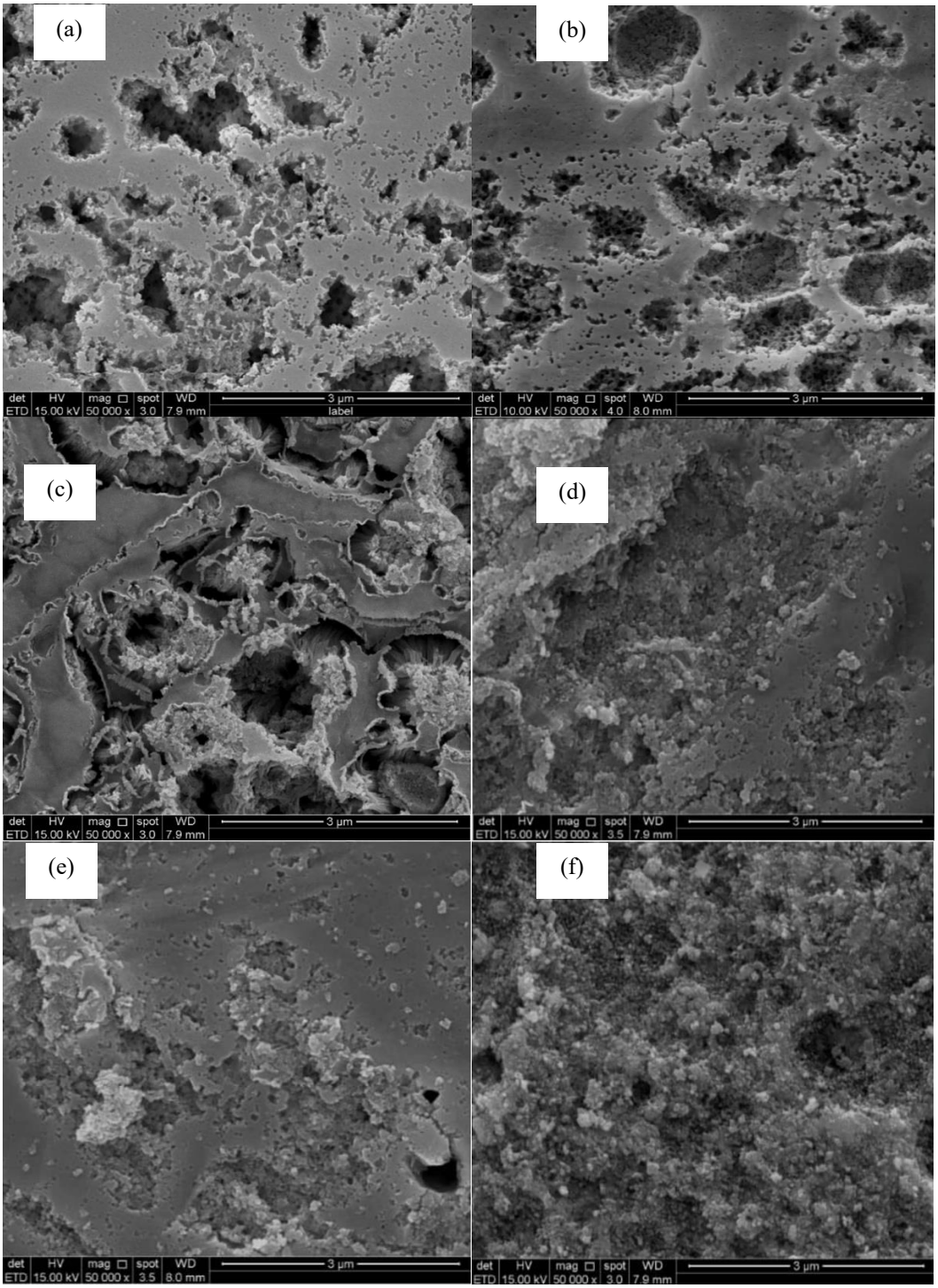

Fig. 3: SEM images of zirconia modified with (a) 0.1 M of $FeSO_4.7H_2O$, (b) 0.5 M of $FeSO_4.7H_2O$ (c) 1.0 M of $FeSO_4.7H_2O$ (d) 0.1 M of $Fe(NO_3)_3.9H_2O$, (e) 0.5 M of $Fe(NO_3)_3.9H_2O$ and (f) 1.0 M of $Fe(NO_3)_3.9H_2O$

https://doi.org/10.24191/esteem.v21iMarch.586.g3074

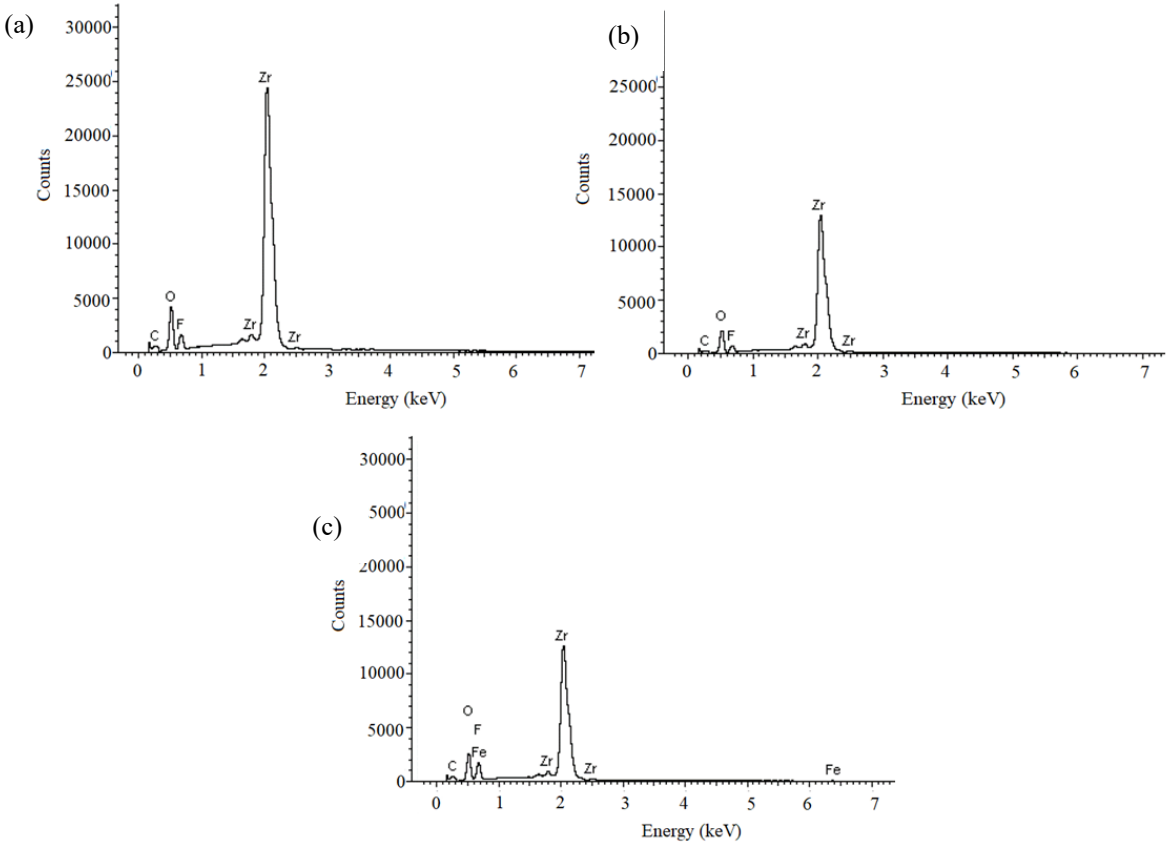

Fig. 4: EDX spectrum of zirconia modified with (a) 0.1 M of $FeSO_4.7H_2O$, (b) 0.5 M of $FeSO_4.7H_2O$ and (c) 1.0 M of $FeSO_4.7H_2O$

https://doi.org/10.24191/esteem.v21iMarch.586.g3074

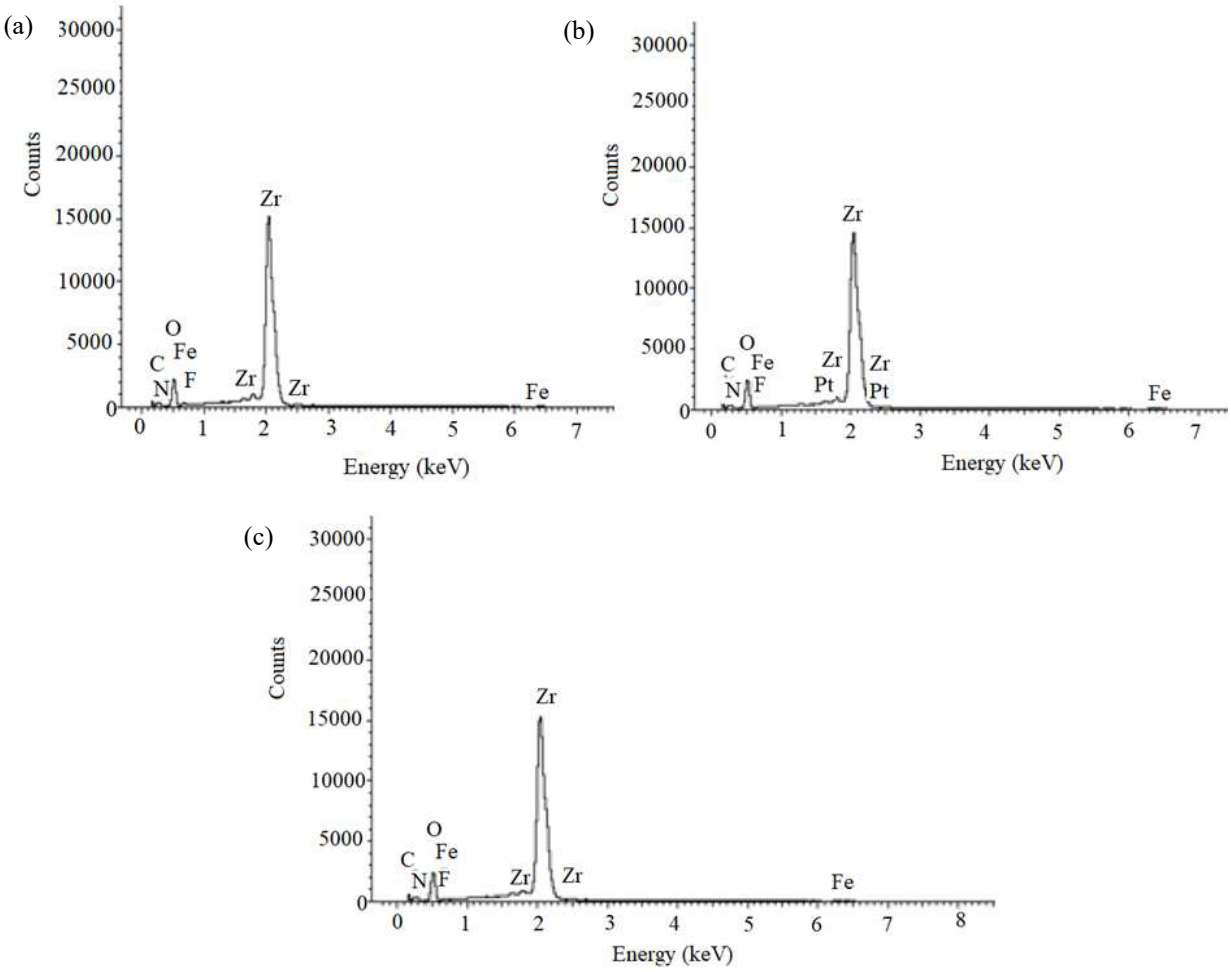

Fig. 5: EDX spectrum of zirconia modified with (a) 0.1 M of $Fe(NO_3)_3.9H_2O$, (b) 0.5 M of $Fe(NO_3)_3.9H_2O$ and (c) 1.0 M of $Fe(NO_3)_3.9H_2$

https://doi.org/10.24191/esteem.v21iMarch.586.g3074

Table 1: EDX data of weight percent composition for iron-doped zirconia at different concentrations type concentrations and types of iron solution.

Sample	Concentration (M)	Element	Weight %
ZrO_2-$FeSO_4.7H_2O$	0.1	C K	5.84
		O K	19.11
		F K	7.45
		Zr L	67.59
	0.5	C K	4.82
		O K	19.64
		F K	6.71
		Zr L	68.83
	1.0	C K	6.91
		O K	18.99
		F K	13.58
		Fe K	0.34
		Zr L	60.19
ZrO_2-$Fe(NO_3)_3.9H_2O$	0.1	C K	6.77
		N K	2.02
		O K	18.83
		F K	1.87
		Fe K	0.17
		Zr L	70.34
	0.5	C K	6.17
		N K	0.87
		O K	20.91
		F K	1.09
		Fe K	0.34
		Zr L	67.74
	1.0	C K	5.34
		N K	1.72
		O K	20.44
		F K	1.00
		Fe K	0.16
		Zr L	71.34

3.2 Comparative with previous study

The modification methods detailed in Table 2 illustrate a variety of approaches for doping ZrO_2 with iron, employing different sources, methods, and concentrations. Significantly, the table reveals that most studies have opted for iron (III) nitrate nonahydrate, $Fe(NO_3)_3 \cdot 9H_2O$, as the preferred iron source for the modification process. This choice indicates the compound's effectiveness in altering the properties of ZrO_2 to enhance its pollutant removal capabilities.

This doping process notably impacts the ability of ZrO_2 to remove a diverse range of pollutants. The types of pollutants studied include organic dyes like rhodamine B, methylene blue, and acid orange, as well as heavy metals such as Cr(VI), arsenate, and uranium, along with other pollutants, including salicylic acid. The performance of ZrO_2 in degrading these pollutants is influenced by the concentration of iron used for doping. According to Table 2, higher iron concentrations often lead to enhanced photocatalytic activity. This suggests a strong correlation between the dopant concentration and the efficiency in pollutant removal.

The prevalent use of iron source for doping, as highlighted in Table 2, underscores its significance in the modification process. This relationship between the type of iron compound used, its concentration, and the resultant photocatalytic efficiency of zirconia is crucial in understanding how iron-doped zirconia can be optimized for environmental applications. This is particularly relevant in water treatment scenarios, where efficiently removing a wide array of pollutants is essential. The choice of $Fe(NO_3)_3 \cdot 9H_2O$ for iron

https://doi.org/10.24191/esteem.v21iMarch.586.g3074

doping, therefore, aligns with the intention to maximize the efficacy of zirconia in such applications, making it a material of high interest for future environmental remediation technologies.

4. CONCLUSION

This study successfully illustrates the significant effect of iron doping on the morphological and compositional features of zirconia foil, showing its increased potential as a photocatalyst. The usage of iron (II) sulfate heptahydrate (**$FeSO_4 \cdot 7H_2O$**) and iron (III) nitrate nonahydrate ($Fe(NO_3)_3.9H_2O$) at varied concentrations has revealed that greater doping levels result in more noticeable physical changes in the material. Even at low concentrations, $Fe(NO_3)_3.9H_2O$ displays effective doping. These findings are critical for expanding the use of zirconia in photocatalysis, laying the groundwork for future research to optimize these materials for environmental and technological applications.

5. ACKNOWLEDGEMENT

This research was supported by Malaysia Ministry of Higher Education – Fundamental Research Grant Scheme FRGS/1/2019/TK05/UNIMAP/03/4 (600-TNCPI/PBT 5/3 (034/2020). The authors also acknowledge the materials, facilities, and financial support provided by University Teknologi MARA, Cawangan Pulau Pinang, for supporting this research.

6. CONFLICT OF INTEREST STATEMENT

The authors agree that this research was conducted in the absence of any self-benefits, commercial or financial conflicts and declare the absence of conflicting interests with the funders.

7. AUTHORS' CONTRIBUTIONS

Nor Aimi Abdul Wahab: Methodology, formal analysis, and writing-original draft; **Adhwa Izzati Md Taib:** Methodology, formal analysis, and writing-original draft, **Nabilah Yasmin Shamsol Afandi:** Methodology, formal analysis, and writing-original draft, **Norain Isa:** Conceptualisation, supervision, editing, and validation, **Nurulhuda Bashirom:** Conceptualisation, supervision, editing, and validation, **Mustaffa Ali Azhar Taib:** Conceptualisation, editing, and validation, **Zainovia Lockman:** Conceptualisation, editing, and validation.

https://doi.org/10.24191/esteem.v21iMarch.586.g3074

Table 2: Comparative study of the effect of iron on modification of zirconia as photocatalyst from the previous study.

Iron Source Used	Iron Concentration	Modification Method	Pollutants	Removal Efficiency (%)	Reaction Time	Observed Effect on Photocatalytic Activity	Ref.
$Fe(NO_3)_3.6H_2O$	0.1, 0.3, 0.5 mol%	Template-free method	Rhodamine B (RhB)	0.3 mol% (81%)	60 min	Incorporating Fe ions led to an increase in the specific surface area and pore volume of the Fe-doped ZrO2 nanoparticles, resulting in improved BET surface area and greater photocatalytic activity than the undoped sample.	[23]
$Fe(NO_3)_3 \cdot 9H_2O$	0.2, 0.5, 2.0, 5.0, 10 mol%	Sol-gel process	Rhodamine B (RhB)	0.5% (96%),	120 min	The photocatalytic activity showed an enhancement in the visible light photocatalytic performance for removing Rhodamine B (RhB)	[31]
$FeCl_3.6H_2O$	5, 10, 50 mol%	Co-precipitation	Cr(VI)	100%	90 min	Fe-doped ZrO_2 exhibits higher photocatalytic activity than ZrO_2 and commercial TiO_2 P25.	[8]
Iron chips	1:1, 1:2, 1:5, 1:10, 1:20, 1:50 and 1:100 molar ratio.	Impregnation	Arsenate (As(V))	98.97%	24 h	The Zr-Fe composite biochar exhibited the highest sorption capacity for As(V) removal compared to the other materials tested.	[32]
$FeCl_3 \cdot 6H_2O$	3, 5, 7, and 10 mol%	Chemical co-precipitation	Methylene blue (MB)	94.2%	120 min	Enhancement in the degradation rate of methylene blue (MB) dye with increasing doping concentration of Fe in the ZrO_2 nanoparticles.	[33]
$Fe(NO_3)_3 \cdot 9H_2O$	0.5 to 4 mol%	Green combustion route	Acid Orange 7 (AO7)	85.0%	90 min	The optimal Fe^{3+} concentration in iron-doped cubic ZrO_2 nanoparticles enhances photocatalytic activity.	[34]
Fe_2O_3	1 Wt %	Sol-gel	Salicylic acid and Cr(VI)	15.8% and 7.0%, for salicylic acid and Cr(VI) pollutants	2 h	Fe^{3+} ion incorporation in the ZrO_2-TiO_2 system negatively impacts its photocatalytic activity for salicylic acid photooxidation and Cr(VI) photoreduction, resulting in lower efficiency than the undoped binary system.	[35]
Zero-valent iron	1:1.25, 1:2.5, and 1:5 feed ratio	Solvothermal	Uranium-contaminated water	91.72%	30 min	The NZVI-PCN-224 photocatalyst effectively reduces U(VI) to U(IV) and maintains a high uranium clearance rate, while also disrupting bacterial and algal cell integrity, making it promising for treating organic water pollutants.	[36]

https://doi.org/10.24191/esteem.v21iMarch.586.g3074

8. REFERENCES

[1] C. Gautam, J. Joyner, A. Gautam, J. Rao, and R. Vajtai, "Zirconia based dental ceramics: structure, mechanical properties, biocompatibility and applications," *Dalt. Trans.*, vol. 45, no. 48, pp. 19194–19215, 2016.

[2] J. Chevalier, L. Gremillard, A. V Virkar, and D. R. Clarke, "The tetragonal-monoclinic transformation in zirconia: lessons learned and future trends," *J. Am. Ceram. Soc.*, vol. 92, no. 9, pp. 1901–1920, 2009.

[3] W. J. Fleming, "Physical principles governing nonideal behavior of the zirconia oxygen sensor," *J. Electrochem. Soc.*, vol. 124, no. 1, p. 21, 1977.

[4] E. D. Jones, "Control of semiconductor conductivity by doping," *Electron. Mater. From Silicon to Org.*, pp. 155–171, 1991.

[5] E.W. Leib, R.M. Pasquarelli, J.J. do Rosário, P.N. Dyachenko, S. Döring, A. Puchert, ... & T. Vossmeyer., "Yttria-stabilized zirconia microspheres: novel building blocks for high-temperature photonics," *J. Mater. Chem. C*, vol. 4, no. 1, pp. 62–74, 2016.

[6] J. Deng, Y. Zhou, S. Li, L. Xiong, J. Wang, S. Yuan, & Y. Chen., "Designed synthesis and characterization of nanostructured ceria-zirconia based material with enhanced thermal stability and its application in three-way catalysis," *J. Ind. Eng. Chem.*, vol. 64, pp. 219–229, 2018, doi: 10.1016/j.jiec.2018.03.018.

[7] A. O. de Souza, F. F. Ivashita, V. Biondo, A. Paesano Jr, and D. H. Mosca, "Structural and magnetic properties of iron doped ZrO_2," *J. Alloys Compd.*, vol. 680, pp. 701–710, 2016.

[8] N. Doufar, M. Benamira, H. Lahmar, M. Trari, I. Avramova, and M. T. Caldes, "Structural and photochemical properties of Fe-doped ZrO_2 and their application as photocatalysts with TiO_2 for chromate reduction," *J. Photochem. Photobiol. A Chem.*, vol. 386, p. 112105, 2020, doi: 10.1016/j.jphotochem.2019.112105.

[9] F. J. Jelaini, N. Bashirom, N. H. N. C. Fauzi, and N. Isa, "Anodic oxidation of Zr-5Fe alloy in ethylene glycol/fluoride electrolyte for Cr(VI) removal under sunlight," *Mater. Today Proc.*, 2023, doi: 10.1016/j.matpr.2023.11.152.

[10] N. Isa, N. Mohamad Nor, W.Z. Wan Kamis, W.K. Tan, G. Kawamura, A. Matsuda, & Z. Lockman., "Anodized TiO_2 nanotubes using Ti wire in fluorinated ethylene glycol with air bubbles for removal of methylene blue dye," *J. Appl. Electrochem.*, vol. 52, no. 1, pp. 173–188, 2022, doi: 10.1007/s10800-021-01644-z.

[11] L. R. Xuen, N. Isa, K. A. Razak, M. Jaafar, and Z. Lockman, "Silver Nanoparticles/Titanium Dioxide Nanowires Photocatalyst Formation for Microplastic Removal Using Ultraviolet Radiation," *Solid State Phenom.*, vol. 352, pp. 67–74, 2023, doi: 10.4028/p-aS0wOb.

[12] N. Bashirom, K. A. Razak, and Z. Lockman, "Synthesis of freestanding amorphous ZrO_2 nanotubes by anodization and their application in photoreduction of Cr(VI) under visible light," *Surf. Coatings Technol.*, vol. 320, pp. 371–376, 2017, doi: 10.1016/j.surfcoat.2016.12.026.

[13] N. Isa, S. H. Sarijo, A. Aziz, and Z. Lockman, "Synthesis colloidal Kyllinga brevifolia -mediated silver nanoparticles at different temperature for methylene blue removal," *AIP Conf. Proc.*, vol. 1877, 2017, doi: 10.1063/1.4999887.

[14] C. Gautam, A. Gautam, V. K. Mishra, N. Ahmad, R. Trivedi, and S. Biradar, "3D interconnected architecture of h-BN reinforced ZrO_2 composites: structural evolution and enhanced mechanical properties for bone implant applications," *Ceram. Int.*, vol. 45, no. 1, pp. 1037–1048, 2019.

[15] B. Z. Janos, E. Lugscheider, and P. Remer, "Effect of thermal aging on the erosion resistance of air plasma sprayed zirconia thermal barrier coating," *Surf. Coatings Technol.*, vol. 113, no. 3, pp. 278–285, 1999.

[16] L. B. Chen, "Yttria-stabilized zirconia thermal barrier coatings—a review," *Surf. Rev. Lett.*, vol. 13, no. 05, pp. 535–544, 2006.

https://doi.org/10.24191/esteem.v21iMarch.586.g3074

[17] R. Kusiorowski, J. Wojsa, B. Psiuk, and T. Wala, "Influence of zirconia addition on the properties of magnesia refractories," *Ceram. Int.*, vol. 42, no. 9, pp. 11373–11386, 2016.

[18] H. P. Beck and C. Kaliba, "On the solubility of Fe, Cr and Nb in ZrO_2 and its effect on thermal dilatation and polymorphic transition," *Mater. Res. Bull.*, vol. 25, no. 9, pp. 1161–1168, 1990.

[19] T. Selvaraj, B. Johar, and S. F. Khor, "Iron/zinc doped 8 mol\% yttria stabilized zirconia electrolytes for the green fuel cell technology: a comparative study of thermal analysis, crystalline structure, microstructure, mechanical and electrochemical properties," *Mater. Chem. Phys.*, vol. 222, pp. 309–320, 2019.

[20] M. Ozawa, "Metal Oxide Materials for Automotive Catalysts," *Nov. Struct. Met. Inorg. Mater.*, pp. 357–367, 2019.

[21] M. Winter and R. J. Brodd, "What are batteries, fuel cells, and supercapacitors?," *Chem. Rev.*, vol. 104, no. 10, pp. 4245–4270, 2004.

[22] T. H. Bui, B. Thangavel, M. Sharipov, K. Chen, and J. H. Shin, "Smartphone-Based Portable Bio-Chemical Sensors: Exploring Recent Advancements," *Chemosensors*, vol. 11, no. 9, p. 468, 2023.

[23] C. V. Reddy *et al.*, "Efficient removal of toxic organic dyes and photoelectrochemical properties of iron-doped zirconia nanoparticles," *Chemosphere*, vol. 239, p. 124766, 2020, doi: 10.1016/j.chemosphere.2019.124766.

[24] N. Isa, T. W. Kian, G. Kawamura, A. Matsuda, and Z. Lockman, "Synthesis of TiO2 Nanotubes Decorated with Ag Nanoparticles (TNTs/AgNPs) for Visible Light Degradation of Methylene Blue," *J. Phys. Conf. Ser.*, vol. 1082, no. 1, 2018, doi: 10.1088/1742-6596/1082/1/012105.

[25] G. Chen, J. J. Peng, C. Song, F. Zeng, and F. Pan, "Interplay between chemical state, electric properties, and ferromagnetism in Fe-doped ZnO films," *J. Appl. Phys.*, vol. 113, no. 10, 2013.

[26] V. G. Neto, C. G. B. Pereira, F. D. Faglioni, C. A. Fortulan, and C. R. Foschini, "ZrO_2-CNT composite production through reducing atmosphere," *Int. J. Adv. Manuf. Technol.*, vol. 122, no. 7, pp. 3323–3335, 2022.

[27] B. Milsom, G. Viola, Z. Gao, F. Inam, T. Peijs, and M. J. Reece, "The effect of carbon nanotubes on the sintering behaviour of zirconia," *J. Eur. Ceram. Soc.*, vol. 32, no. 16, pp. 4149–4156, 2012.

[28] G. Xu, Y.-W. Zhang, C.-S. Liao, and C.-H. Yan, "Doping and grain size effects in nanocrystalline ZrO_2-Sc_2O_3 system with complex phase transitions: XRD and Raman studies," *Phys. Chem. Chem. Phys.*, vol. 6, no. 23, pp. 5410–5418, 2004.

[29] B. Fan, Z. Zhang, C. Liu, and Q. Liu, "Investigation of sulfated iron-based catalysts with different sulfate position for selective catalytic reduction of NOx with NH_3," *Catalysts*, vol. 10, no. 9, p. 1035, 2020.

[30] C. Fletcher, Y. Jiang, C. Sun, and R. Amal, "Morphological evolution and electronic alteration of ZnO nanomaterials induced by Ni/Fe co-doping," *Nanoscale*, vol. 6, no. 13, pp. 7312–7318, 2014.

[31] Q. Cheng, W. Yang, Q. Chen, J. Zhu, D. Li, L. Fu, & L. Zhou., "Fe-doped zirconia nanoparticles with highly negative conduction band potential for enhancing visible light photocatalytic performance," *Appl. Surf. Sci.*, vol. 530, p. 147291, 2020, doi: 10.1016/j.apsusc.2020.147291.

[32] M.A. Rahman, D. Lamb, M.M. Rahman, M.M. Bahar, P. Sanderson, S. Abbasi, ... & R. Naidu.., "Removal of arsenate from contaminated waters by novel zirconium and zirconium-iron modified biochar," *J. Hazard. Mater.*, vol. 409, 2020, p. 124488, 2021, doi: 10.1016/j.jhazmat.2020.124488.

[33] W. Ahmed, J. Iqbal, S.O. Aisida, A. Badshah, I. Ahmad, K. Alamgir, & I.H. Gul., "Structural, magnetic and dielectric characteristics of optically tuned Fe doped ZrO_2 nanoparticles with visible light driven photocatalytic activity," *Mater. Chem. Phys.*, vol. 251, no. October 2019, p. 122999, 2020, doi: 10.1016/j.matchemphys.2020.122999.

[34] K. Gurushantha, K.S. Anantharaju, H. Nagabhushana, S.C. Sharma, Y.S. Vidya, C. Shivakumara, ... & M.R. Anilkumar., "Facile green fabrication of iron-doped cubic ZrO_2 nanoparticles by Phyllanthus acidus: Structural, photocatalytic and photoluminescent properties," *J. Mol. Catal. A Chem.*, vol. 397, pp. 36–47, 2015, doi: 10.1016/j.molcata.2014.10.025.

https://doi.org/10.24191/esteem.v21iMarch.586.g3074

[35] M. C. Hidalgo *et al.*, "EXAFS study and photocatalytic properties of un-doped and iron-doped ZrO_2-TiO_2 (photo-) catalysts," *Catal. Today*, vol. 128, no. 3-4 SPEC. ISS., pp. 245–250, 2007, doi: 10.1016/j.cattod.2007.07.010.

[36] J. Zhao, C. Lyu, R. Zhang, Y. Han, Y. Wu, and X. Wu, "Self-cleaning and regenerable nano zero-valent iron modified PCN-224 heterojunction for photo-enhanced radioactive waste reduction," *J. Hazard. Mater.*, vol. 442, 2022, p. 130018, 2023, doi: 10.1016/j.jhazmat.2022.130018.

https://doi.org/10.24191/esteem.v21iMarch.586.g3074